



Synthesis and characterization of Y and Dy co-doped ceria solid electrolytes for IT-SOFCs: a microwave sintering

Ch. Madhusudan*[✉], Venkataramana Kasarapu, Madhuri Chittimadula,
Y. Suresh Reddy, C. Vishnuvardhan Reddy

Received: 10 October 2017/Revised: 18 November 2017/Accepted: 18 April 2018/Published online: 15 May 2018
© The Nonferrous Metals Society of China and Springer-Verlag GmbH Germany, part of Springer Nature 2018

Abstract In this communication, the electrical conductivities and thermal expansion studies of microwave sintered co-doped ceria $\text{Ce}_{0.8}\text{Y}_{0.2-x}\text{Dy}_x\text{O}_{2-\delta}$ ($x = 0, 0.05, 0.10, 0.15$ and 0.20) solid electrolyte materials for intermediate temperature solid oxide fuel cells (IT-SOFCs) synthesized by sol-gel auto-combustion method were discussed. Microwave sintering at $1300\text{ }^\circ\text{C}$ for 30 min was used for making dense powder compacts. The relative densities of all the samples are noticed above 95%. Raman spectrum was characterized by the presence of a very strong band near 460 cm^{-1} , which along with X-ray diffraction (XRD) analysis ascertain the sample formation with a single-phase cubic fluorite structure. The lattice parameter values were calculated from XRD patterns. SEM images show nearly uniform grains with distinct grain boundaries. The thermal expansion coefficients (TECs) are found to vary linearly with temperature and were measured in the range from 14.15 to $13.20 \times 10^{-6}\text{ }^\circ\text{C}^{-1}$. The investigation on total ionic conductivity (TIC) was executed with variation in dopant concentration and relative oxygen vacancies. The impedance analysis reveals that the sample $\text{Ce}_{0.80}\text{Y}_{0.10}\text{Dy}_{0.10}\text{O}_{2-\delta}$ displays the highest TIC, i.e., $7.5 \times 10^{-3}\text{ S}\cdot\text{cm}^{-1}$ at $500\text{ }^\circ\text{C}$ and minimum activation energy 0.90 eV compared to others. With the highest TIC and minimum activation energy, the $\text{Ce}_{0.80}\text{Y}_{0.10}\text{Dy}_{0.10}\text{O}_{2-\delta}$ might be the possible material as the solid electrolyte in intermediate temperature SOFCs.

Keywords Microwave sintering; Ionic conductivity; Co-doped ceria; Solid electrolyte; Intermediate temperature solid oxide fuel cells

1 Introduction

The emergence of solid oxide fuel cells (SOFCs) as vital alternate energy conversion systems is imperative in reducing emissions and impacting the environmental emissions such as CO_x , NO_x , SO_x and their impact in global warming. Among the present day varied fuel cell technologies, this has the ability to convert the chemical energy into electrical energy with high conversion efficiency and fuel flexibility [1–4].

Yttria-stabilized zirconia (YSZ), which is a popular traditional electrolyte material for SOFC, requires higher operating temperatures ($> 1000\text{ }^\circ\text{C}$) to exhibit high ionic conductivity. The high operating temperature is one of the major barriers which still hamper the development and commercialization of SOFCs. SOFCs that can be operated at intermediate temperatures ($500\text{--}800\text{ }^\circ\text{C}$) may have many benefits in terms of fabrication-operation costs, cell material selection and the life span that is only limited by a mismatch in thermal expansion rates or a side reaction between adjacent cell parts [5, 6].

A single fuel cell consists of an electrolyte sandwiched between two thin electrodes (porous anode and cathode). Solid electrolyte is the key component of SOFC, which would be a humdinger in SOFC applications in perspective that it affects the operating temperature. Unlike other fuel cells, the SOFCs conduct oxygen ions from the cathode to the anode through the electrolyte, and hydrogen or carbon monoxide reacts with the oxygen ions in the anode [3, 4].

Ch. Madhusudan*, V. Kasarapu, M. Chittimadula,
Y. S. Reddy, C. V. Reddy
Department of Physics, Osmania University, Hyderabad,
Telangana 500007, India
e-mail: maduoumadu@gmail.com

Much research work has been focused on new SOFC electrolyte materials which can be operated in the intermediate temperature range. This would be a potential replacement for YSZ electrolyte. Fluorite structured cerium oxide (ceria)-based solid electrolytes have been widely investigated thanks to their growing demand in IT-SOFCs, as they have high ionic conductivity compared to YSZ at relatively low operating temperatures. Studies on ceria are being conducted extensively for its ability to store and release oxygen ion vacancies due to its easily accessible oxidation states from $Ce^{3+} \rightleftharpoons Ce^{4+}$ and hence will have high ionic conductivity due to oxygen vacancies [7, 8]. For this reason, pure ceria necessitates structural modification to accommodate significantly a large number of oxygen vacancies to enhance high ionic conductivity [9]. The ionic conductivity of doped ceria electrolyte may depend on several factors like dopant ions and their radii, dopant concentration, oxygen vacancies and local defect structures [10–12]. Researchers used various structural and technological modifications through doping viz. grain size reduction, development of multi-phase materials and multilayered thin films of cerium oxide-based electrolytes, showing an improvement in ionic conductivity [13]. Addition of co-dopant into the lattice of solid ceria electrolytes at intermediate temperatures reported high ionic conductivity compared to single doped ceria [14–18]. Recently, some co-doped ceria electrolytes have been extensively investigated such as, $Ce_{1-x}Sm_xMg_yO_{2-\delta}$ [16], $Ce_{1-x}(Gd_{0.5}Pr_{0.5})O_2$ [19], $Ce_{0.8}Sm_{0.12}Pr_{0.08}O_{2-\delta}$ [20], $Ce_{0.85}Gd_{0.1}Sm_{0.05}O_{1.925}$ [21], $Ce_{0.85}Sm_{0.1}Nd_{0.05}O_{2-\delta}$ [22], $Ce_{1-x}(Pr_{1/3}Sm_{1/3}Gd_{1/3})_xO_{2-\delta}$ [23] and reported considerable improvement in total ionic conductivity (TIC) due to the presence of oxygen vacancies in ceria. Zivkovic et al. [7], Peng et al. [9], Lopez et al. [24], Li et al. [25] and others studied the Raman spectroscopy to correlate the ionic conductivity and the presence of oxygen vacancies and reported that the existence of high concentration of oxygen vacancies caused the greater ionic conductivity of the sample.

In order to be an efficient electrolyte material, ceria must also have a matching thermal expansion coefficient (TEC) with the cathode and anode materials in between which it is sandwiched. Otherwise, it may result in unwanted stress during the fabrication and operation and may develop micro-cracks in ceramic structure, leading to a thermally unstable SOFC [26, 27]. TEC depends on the ionic radius of dopant, dopant concentration and lattice parameter [28]. Densification of the electrolyte material at lower sintering temperatures still remains as one of the major technical challenges which can save energy and reduce the fabrication costs of SOFCs. Of late, microwave sintering (MS) of ceramics has emerged as an alternative approach for densification of ceramics and has become a

most sought-after process due to its rapid heating, enhanced densification rate yielding in uniform and finer microstructure with much better densities at lower temperatures compared to conventional sintering due to homogenous temperature distribution, both on the surface as well as in the core during MS [29].

Earlier, Tadokoro et al. [30] investigated $Ce_{1-x}(Y_{0.5}Dy_{0.5})_xO_{2-\delta}$ ($0 \leq x \leq 0.15$) system synthesized via co-precipitation method with conventional sintering at 1450 °C for 4 h and reported structural and electrical properties. In this work, it was investigated the structural, electrical and thermal properties of yttrium and dysprosium co-doped ceria system $Ce_{0.8}Y_{0.2-x}Dy_xO_{2-\delta}$ ($x = 0, 0.05, 0.10, 0.15$ and 0.20) synthesized via sol-gel auto-combustion method. The energy efficient fritage, the microwave sintering which has several advantages over the traditional sintering, was used, and a co-doped solid ceria electrolyte which may be a potential electrolyte for intermediate temperature solid oxide fuel cells (IT-SOFCs) was developed.

2 Experimental

2.1 Materials and methods

The Y^{3+} and Dy^{3+} co-doped ceria $Ce_{0.8}Y_{0.2-x}Dy_xO_{2-\delta}$ ($x = 0, 0.05, 0.10, 0.15$ and 0.20) electrolyte materials were synthesized via sol-gel auto-combustion synthesis [14]. As initial ingredient such as stoichiometric proportions of ammonium ceric nitrate, yttrium nitrate hex hydrate, dysprosium nitrate hex hydrate, citric acid, ethylene glycol and ammonia solution were weighed and dissolved in deionized water. Citric acid and ethylene glycol were added to the resultant solution with metal to citric acid ratio as 1:1.5 and citric acid to ethylene glycol ratio as 1:1.2. The mixture was stirred with magnetic stirrer to ensure that the solution is homogeneous. Ammonia was added drop by drop to the mixture in order to adjust the pH ($pH = 7$). The final homogeneous solution was heated to nearly 100 °C to evaporate the water and excess residues for forming viscous gel like substance. The obtained gel was further heated to 150 °C for reaching the combustion point. In a few minutes, it produced solid particles. These particles were ground thoroughly in the agate mortar. The powder thus ground was calcined for 2 h at 800 °C to eliminate unwanted carbonaceous materials and also to get crystallized formation of samples. The calcined powders were further ground and were compressed with a pellet die at a pressure of 5 MPa to give pellets with dimensions of 10 mm in diameter and 2 mm in thickness each. The dense pellets were obtained by sintering at 1300 °C for 30 min using a programmable microwave furnace.

2.2 Characterization

All the samples were characterized at room temperature by powder X-ray diffractometer (XRD, Philips Xpert PRO ALPHA1) with Cu K α 1 monochromatic radiation ($\lambda = 0.15406$ nm) in phase-wise analysis. XRD patterns were noticed in 2θ range of 20° – 80° with a step size of 0.02° at the scanning rate of $2^\circ \cdot \text{min}^{-1}$. The microstructure and analysis of elemental composition of sintered samples were executed by scanning electron microscope (SEM) and energy-dispersive spectrum (EDS) using ZEISS EVO 18 special edition. To enable SEM characterization, the prepared pellets were sputtered with Au coating. Structural analysis was carried out by Raman spectroscopy using Horiba–Jobin–Yvon micro-Raman spectrometer. Impedance measurements of all the samples were taken using the Wayne Kerr impedance analyzer 6500B with temperatures ranging from 250 to 500 °C. Netzsch DIL 402 PC dilatometer was used to investigate the thermal expansion studies of $\text{Ce}_{0.8}\text{Y}_{0.2-x}\text{Dy}_x\text{O}_{2-\delta}$ in the temperatures ranging from room temperature to 800 °C at a heating rate of $3^\circ \cdot \text{min}^{-1}$.

3 Results and discussion

3.1 XRD analysis

XRD patterns of all the $\text{Ce}_{0.8}\text{Y}_{0.2-x}\text{Dy}_x\text{O}_{2-\delta}$ powder samples recorded at room temperature are presented in Fig. 1a. These XRD patterns of all the obtained co-doped ceria show the typical cubic fluorite structure of $Fm\bar{3}m$ space group which coincides well with the standard data of CeO_2 [JCPDS PDF No. 34–0394]. It can also be observed from Fig. 1a that all the XRD patterns are of single phase. The diffraction peaks corresponding to (111), (200), (220), (311), (222), (400), (331) and (420) are observed. Shifting

of position of peaks is also observed, as shown in Fig. 1b, with the (111) diffraction peaks shifting to the left or smaller 2θ with the increase in the dopant concentration. Table 1 shows the variation of lattice parameters for different compositions (with different dopant concentrations) of the obtained co-doped ceria with the shifts in diffraction peaks. The observed lattice parameters are found to increase with linear dependency on the dopant composition (with different dopant concentrations); the change in the lattice parameter values is due to the difference between the ionic radius of dopants ($r(\text{Y}^{3+}) = 0.1019$ nm, $r(\text{Dy}^{3+}) = 0.1027$ nm) [31]. The other crystallographic data such as structure, unit cell volume and relative density of co-doped ceria system are also presented in Table 1.

The bulk density (D) of the sintered pellets were measured using the Archimedes principle, the theoretical density (D_{th}) was calculated based on XRD data, and the relative density (D_{rel}) was calculated as the ratio of bulk density to theoretical density.

$$D_{\text{rel}} = \frac{D}{D_{\text{th}}} \times 100\% \quad (1)$$

The relative densities of all the samples were found to be in the range of 96 and 97.5%. This indicated the low porosity in the co-doped ceria samples.

3.2 Microstructure

The morphology of dense pellets microwave sintered at 1300 °C for 30 min obtained by SEM shows their microstructure. SEM images and EDS profile of all the Au coated co-doped ceria samples with additives of different proportions are shown in Fig. 2. The co-doped ceria samples $\text{Ce}_{0.8}\text{Y}_{0.2-x}\text{Dy}_x\text{O}_{2-\delta}$ show very dense structure. Microwave sintering at 1300 °C yields a near uniform sub-micrometer grain size with negligible porosity. EDS results in Fig. 2 confirm the presence of Ce, Y, Dy and O in all the

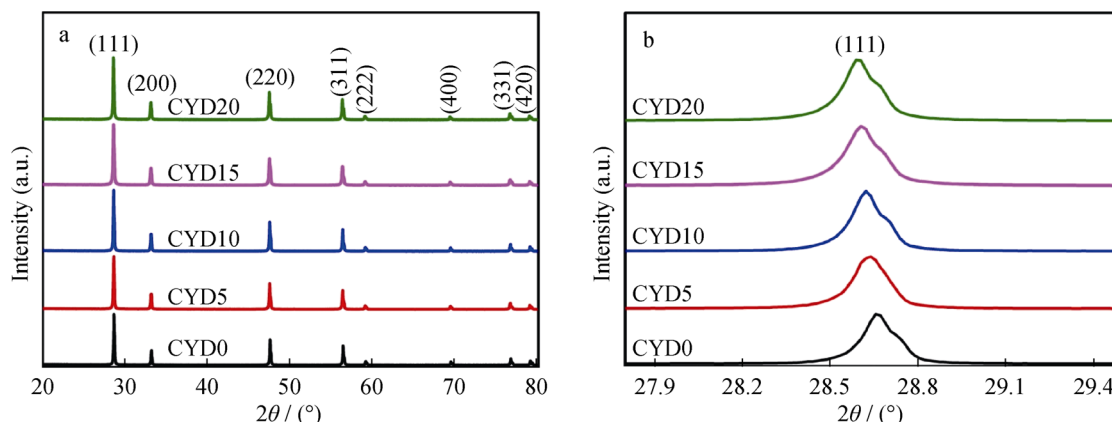


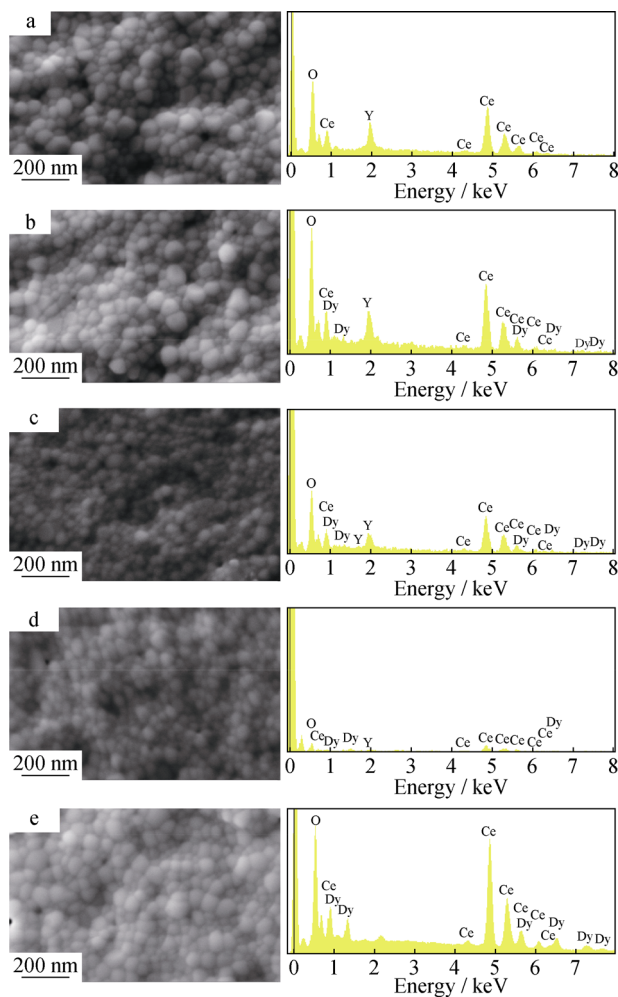
Fig. 1 a XRD patterns of CYD system and b peak shift in PXRD patterns of CYD system

Table 1 Crystallographic parameters of CYD system

Samples	Crystal structure	Lattice parameter/nm	Volume/ nm ³	Relative density/%
CYD0	Cubic	5.4010	0.15755	95.4
CYD5	Cubic	5.4029	0.15772	96.3
CYD10	Cubic	5.4046	0.15787	97.1
CYD15	Cubic	5.4070	0.15808	96.8
CYD20	Cubic	5.4083	0.15820	96.4

Table 2 Elemental composition (EDS analysis) of CYD system (at%)

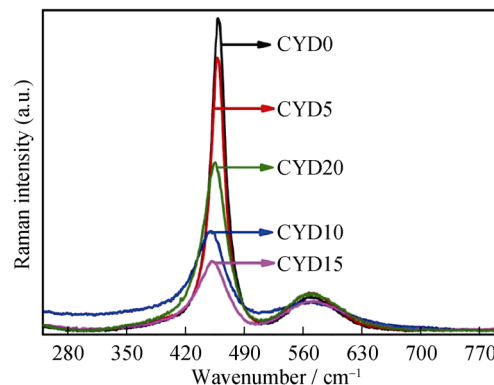
Samples	Ce	Y	Dy	O
CYD0	26.61	6.67	–	66.72
CYD5	26.46	5.11	1.48	66.95
CYD10	27.12	3.47	3.53	65.88
CYD15	27.08	1.71	5.14	66.07
CYD20	26.86	–	6.75	66.39

**Fig. 2** SEM images and EDS spectra of CYD system: **a** CYD0, **b** CYD05, **c** CYD10, **d** CYD15, and **e** CYD20

compositions, and no other elements are observed. Table 2 depicts the elemental content of each composition of the denser pellets obtained.

3.3 Raman spectroscopy

Raman spectra of all the microwave sintered $\text{Ce}_{0.8}\text{Y}_{0.2-x}\text{Dy}_x\text{O}_{2-\delta}$ samples are shown in Fig. 3. Raman spectroscopic studies were the vital tools for analyzing the

**Fig. 3** Raman spectra of CYD system

presence of functional groups in the chemical composition of the samples. It displays the sensitivity to identify the presence of oxygen vacancies in co-doped ceria lattice, which corroborates with XRD and TIC data [24–27]. The Raman spectrum of the obtained co-doped ceria is dominated by F_{2g} band at 460 cm^{-1} which is the characteristic peak for fluorite structure of ceria. This means that all dopants are partially substituted to Ce^{4+} of crystal lattice of CeO_2 , which also confirms the formation of $\text{Ce}_{0.8}\text{Y}_{0.2-x}\text{Dy}_x\text{O}_{2-\delta}$ solid solution [9]. In addition to the strong F_{2g} band, yttrium and dysprosium co-doped ceria shows a weaker intense peak positioned at 570 cm^{-1} . This weaker peak appeared at 570 cm^{-1} is attributed to extrinsic oxygen vacancies in ceria [30]. The mode at 570 cm^{-1} associated with the extrinsic oxygen vacancy is induced by the doping of CeO_2 . The ratio of area of stronger peak to the area of weaker peak (i.e., A_{570}/A_{460}) at full width half maximum (FWHM) and the values of intensity ratios (i.e., I_{570}/I_{460}) of all the compositions were calculated and are listed in Table 3 [24]. From Table 3, it can be seen that the $\text{Ce}_{0.8}\text{Y}_{0.10}\text{Dy}_{0.10}\text{O}_{2-\delta}$ is found to have high value of FWHM, intensity ratio and area ratio, confirming the high concentration of O^{2-} vacancies in the composition [7]. Owing to the high concentration of oxygen vacancies, one can expect the highest TIC in $\text{Ce}_{0.8}\text{Y}_{0.10}\text{Dy}_{0.10}\text{O}_{2-\delta}$ composition among all the samples. The formation of this co-

Table 3 Parameters of Raman analysis for CYD system

Samples	FWHM ₄₆₀	A ₅₇₀ /A ₄₆₀
CYD0	22.10	0.31
CYD5	22.52	0.43
CYD10	39.76	1.01
CYD15	38.90	0.85
CYD20	35.10	0.44

doped ceria system of materials prepared through the sol-gel auto-combustion synthesis is confirmed by XRD, SEM and EDS results along with the Raman spectra results.

3.4 Electrochemical impedance spectroscopy (EIS) results

EIS or simply impedance spectroscopy was the powerful electrochemical perturbation alternative current (AC) technique used to study the electrical properties of solid electrolytes. The usefulness of impedance spectroscopy lies in the ability to distinguish the dielectric and electric properties of individual contributions of components under investigation. Impedance data collected for the obtained samples were graphed in a Nyquist plots. A Nyquist plot was graphed with real part of the impedance (Z') on x -axis and negative imaginary part of impedance ($-Z''$) on y -axis [32, 33]. Nyquist plot of an electrolyte material characterized by three successive semicircular arcs: high frequency semicircle corresponding to grain resistance (R_g), intermediate frequency semicircle corresponding to grain boundary resistance (R_{gb}) and low-frequency incomplete arc corresponding to electrode resistance (R_e) [19, 34, 35].

The impedance analysis of all the specimens was performed in the temperatures ranging from 250 to 500 °C with the frequency range of 50 Hz–5 MHz, as shown in Fig. 4. The complex impedance plots of all the compositions were fitted by Z-View software. Impedance spectra were fitted to equivalent circuits, which consist of three parallel resistances (R) and constant phase elements (CPEs) connected in series. CPE has been used in place of ideal capacitor due to the presence of inhomogeneities of ceria-based materials. CPE was equivalent to the distribution of capacitors in parallel [19, 36]. It can be observed that the radius of the semicircle decreases with the increase in the composition up to $x = 0.10$ co-doping on ceria and then increases. At high temperatures, there is a decrease in impedance and semicircles shift toward higher frequency side.

3.5 TIC analysis

The total ionic conductivity, TIC (σ_t), was then calculated by the following equation:

$$\sigma_t = \frac{l}{R_t A} \quad (2)$$

where l is the specimen thickness, R_t is the total resistance of the specimen and A is cross-sectional area of the specimen. The total resistance (R_t) of the specimens includes the grain resistance (R_g) and grain boundary resistance (R_{gb}) from the complex impedance.

Table 4 shows the values of grain conductivity (σ_g), grain boundary conductivity (σ_{gb}) and the total ionic conductivity (σ_t) values. It can be seen from Fig. 4a, b and Table 4 that the TIC is found to be increasing with the increase in the concentration of dopants. This trend follows up to $x = 0.10$ (i.e., 10 mol% Y and Dy) and then decreases at higher doping concentration. The highest TIC is observed for $\text{Ce}_{0.8}\text{Y}_{0.10}\text{Dy}_{0.10}\text{O}_{2-\delta}$ ($7.5 \times 10^{-3} \text{ S}\cdot\text{cm}^{-1}$) at 500 °C. The increase in the concentration of mobile ions (oxygen vacancies) leads to the enhanced ionic conductivity of the co-doped ceria. The decreased mobile oxygen vacancies lead to the decrease in TIC due to formation of local defects in the ceria structure [14, 15, 37].

Figure 5a–c displays the grain, grain boundary and total conductivities of the samples expressed in the form of Arrhenius plots in the temperatures ranging from 250 to 500 °C. These temperature-dependent conductivity plots may be linearized by plotting the logarithmic relation between $\lg\sigma T$ and $1000/T$ [15, 37]. The activation energy for conduction of all samples was calculated from the conductivity plots by using Arrhenius relation,

$$\sigma T = \sigma_0 \exp\left(-\frac{E}{KT}\right) \quad (3)$$

where E is the activation energy for conduction (ion migration), T indicates the absolute temperature, K represents the Boltzmann constant, and σ_0 denotes the pre-exponential factor. The activation energies of grain (E_a^g), grain boundary (E_a^{gb}) and total (E_a^t) for ionic conduction were calculated and are listed in Table 5. The minimum activation energy of 0.90 eV is achieved for the composition $x = 0.10$. The presence of mobile oxygen vacancies (defects) causes the interaction between the dopant cations and results in smaller calculated activation energies [15].

From Raman spectroscopy analysis (Table 3), it is concluded that the high values of FWHM, I_{570}/I_{460} and A_{570}/A_{460} confirm the formation of high concentration of oxygen vacancies which cause the mobilization of ions in the ceria lattice yielding the best TIC of $7.5 \times 10^{-3} \text{ S}\cdot\text{cm}^{-1}$ with less activation energy of 0.90 eV in $\text{Ce}_{0.8}\text{Y}_{0.10}\text{Dy}_{0.10}\text{O}_{2-\delta}$ at 500 °C.

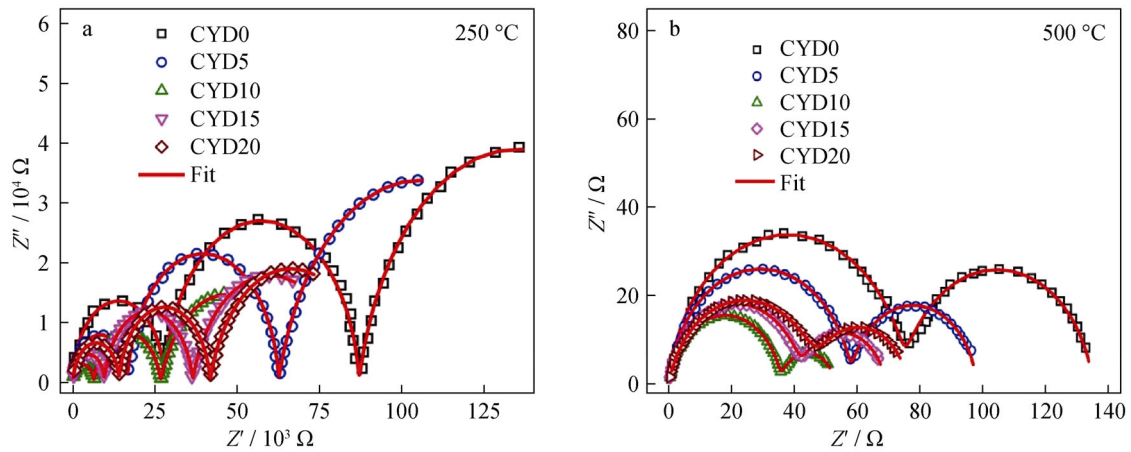


Fig. 4 Complex impedance plots of CYD system at **a** 250 °C and **b** 500 °C

3.6 Thermal expansion studies

In order to be an efficient electrolyte, ceria must also have a matching TEC with interconnection and the electrode materials (anode and cathode) in between which it was sandwiched in addition to its high ionic conductivity. Mismatching of TEC might result in unwanted stress during the fabrication and operation and may develop cracks in ceramic structure, leading to a transient thermal unstable SOFC. The TEC depends on electrostatic forces within the lattice, i.e., the thermal expansion varies inversely with

the electrostatic forces (thermal expansion depends on concentration and relative separation of positive and negative charges in the lattice) [23, 38, 39]. Thermal expansion curves of the composites $\text{Ce}_{0.8}\text{Y}_{0.2-x}\text{Dy}_x\text{O}_{2-\delta}$ are shown in Fig. 6. The linear thermal expansion (dL/L_0) for all the samples obtained was calculated in the temperature range of 30–800 °C. The TEC was calculated from the expansion curves for microwave sintered $\text{Ce}_{0.8}\text{Y}_{0.2-x}\text{Dy}_x\text{O}_{2-\delta}$ using the following equation.

$$\text{TEC} = \frac{dL/L_0}{dT} = \frac{(L - L_0)/L_0}{T - T_0} \quad (4)$$

Table 4 Conductivity values at 500 °C for CYD system ($\text{S}\cdot\text{cm}^{-1}$)

Samples	σ_g	σ_{gb}	σ_t
CYD0	0.0053	0.0067	0.0030
CYD5	0.0069	0.0100	0.0041
CYD10	0.0110	0.0230	0.0075
CYD15	0.0091	0.0150	0.0056
CYD20	0.0082	0.0130	0.0052

Table 5 Activation energies (E_a) for CYD system (eV)

Samples	E_a^g	E_a^{gb}	E_a^t
CYD0	0.86	1.03	0.97
CYD5	0.85	1.02	0.95
CYD10	0.78	0.96	0.90
CYD15	0.82	1.00	0.91
CYD20	0.84	0.97	0.92

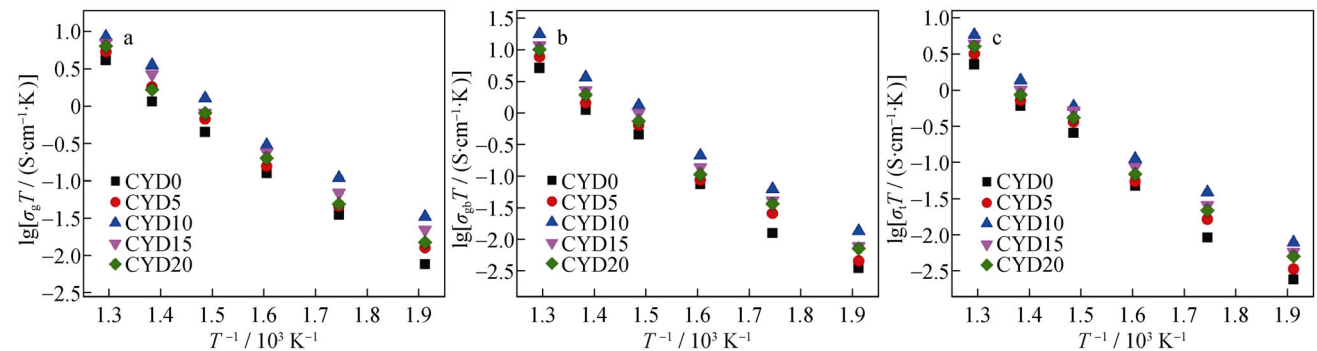


Fig. 5 Temperature-dependent **a** grain conductivity, **b** grain boundary conductivity and **c** total conductivity of CYD system

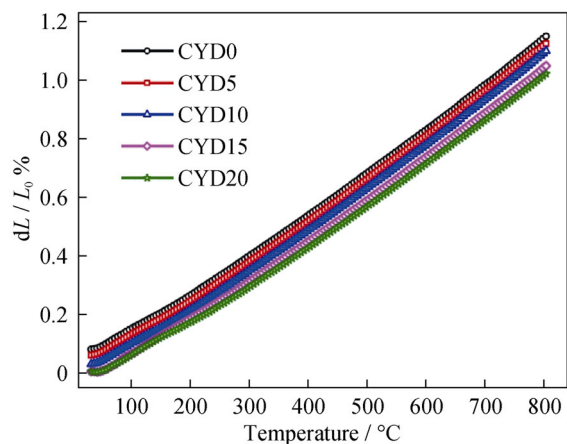


Fig. 6 Thermal expansion curves of CYD system

Table 6 Coefficients of thermal expansion (CTE) for CYD system ($10^{-6} \text{ } ^\circ\text{C}^{-1}$)

Samples	RT-600 $^\circ\text{C}$	RT-800 $^\circ\text{C}$
CYD0	13.67	14.15
CYD5	13.14	13.95
CYD10	12.95	13.42
CYD15	12.67	13.35
CYD20	12.55	13.20

where L_0 is the length at initial temperature (T_0) and L is the length at terminal temperature (T) of the experiment. From Table 6, it can be seen that the calculated TEC values of these co-doped ceria material are in good concurrence with the literature. Furthermore, the Y^{3+} and Dy^{3+} co-doped ceria $\text{Ce}_{0.8}\text{Y}_{0.2-x}\text{Dy}_x\text{O}_{2-\delta}$ materials show good compatibility with the TECs of electrode materials [27, 40–44]. The high TIC and thermal compatibility make the co-doped ceria material $\text{Ce}_{0.80}\text{Y}_{0.10}\text{Dy}_{0.10}\text{O}_{2-\delta}$ investigated in the present work as a potential candidate in IT SOFC.

4 Conclusion

The Y and Dy co-doped ceria $\text{Ce}_{0.8}\text{Y}_{0.2-x}\text{Dy}_x\text{O}_{2-\delta}$ electrolyte materials were successfully synthesized by sol-gel auto-combustion method. The energy efficient microwave sintering results in high relative densities ($> 95\%$) of the obtained pellets. XRD patterns and Raman spectra of all the samples ascertain the formation of single-phase cubic fluorite structure. The morphology was analyzed by SEM and the composition of elements was confirmed by EDS. The calculated linear TECs of all the samples are in good agreement with the commonly used electrode materials for

IT-SOFCs. The formation of oxygen vacancies is confirmed by Raman spectroscopy in the investigated co-doped ceria, and the concentration of oxygen vacancies was evaluated using Raman spectra. High concentration of oxygen vacancies is found in $\text{Ce}_{0.80}\text{Y}_{0.10}\text{Dy}_{0.10}\text{O}_{2-\delta}$. The impedance measurements show the highest TIC of $7.5 \times 10^{-3} \text{ S}\cdot\text{cm}^{-1}$ with a minimum activation energy of 0.90 eV for the composition $\text{Ce}_{0.80}\text{Y}_{0.10}\text{Dy}_{0.10}\text{O}_{2-\delta}$ at 500 $^\circ\text{C}$. Finally, it is concluded that the co-doped ceria material $\text{Ce}_{0.80}\text{Y}_{0.10}\text{Dy}_{0.10}\text{O}_{2-\delta}$ would be an excellent choice as an electrolyte in IT-SOFCs.

Acknowledgements This work was financially supported by the University Grants Commission, New Delhi, India, under the scheme of Faculty Development Program (No. Lr. APKA028/001/XIIPLAN).

References

- [1] Burbano M, Nadin S, Marrocchelli D, Salanne M, Watson GW. Ceria co-doping synergistic or average effect? *Phys Chem Chem Phys.* 2014;16(18):8320.
- [2] Faro ML, La Rosa D, Antonucci V. Intermediate temperature Solid oxide fuel electrolytes. *J Indian Inst Sci.* 2009;89(4):363.
- [3] Kreuer KD. *Fuel Cells, Introduction.* New York: Springer; 2013. 1.
- [4] Huijsmans JPP, van Berkel FPF, Christie GM. Intermediate temperature SOFC—a promise for the 21st century. *J Power Sources.* 1998;71(1–2):107.
- [5] Brett DJL, Atkinson A, Brandon NP, Skinner SJ. Intermediate temperature solid oxide fuel cells. *Chem Soc Rev.* 2008;37: 1568.
- [6] Ralph JM, Schoeler AC, Krumpelt M. Materials for lower temperature solid oxide fuel cells. *J Mater Sci.* 2001;36(5):1161.
- [7] Zivkovic LJS, Lair V, Lupan O, Cassir M, Ringuede A. Samarium-doped ceria nanostructured thin films grown on FTO glass by electrodeposition. *Acta Phys Pol, A.* 2011;120:298.
- [8] Otake T, Yugami H, Yashiro K, Nigara Y, Kawada T, Mizusaki J. Nonstoichiometry of $\text{Ce}_{1-x}\text{Y}_x\text{O}_{2-0.5x-\delta}$ ($X = 0.1, 0.2$). *Solid State Ionics.* 2003;161(1–2):181.
- [9] Peng C, Wang Y, Jiang K, Bin BQ, Liang HW, Feng J, Meng J. Study on the structure change and oxygen vacation shift for $\text{Ce}_{1-x}\text{Sm}_x\text{O}_{2-y}$ solid solution. *J Alloy Compd.* 2003;349(1–2): 273.
- [10] Acharya SA, Gaikwad VM, D'Souza SW, Barman SR. Gd/Sm dopant-modified oxidation state and defect generation in nano-ceria. *Solid State Ionics.* 2014;260:21.
- [11] Matovic B, Pantic J, Lukovic J, Ilic S, Stabkovic N, Kokunsovski M, Miljevic M. Synthesis and characterization of (Ba, Yb) doped ceria nanopowders. *Process Appl Ceram.* 2011;5(2): 69.
- [12] Ganduglia-Pirovano MV. Oxygen defects at reducible oxide surfaces: the example of ceria and vanadia. In: Jupille J, Thornton G, editors. *Defects at Oxide Surfaces.* Berlin: Springer International Publishing; 2015. 149.
- [13] Liu YY, Fan LD, Cai YX, Zhang W, Wang BY, Zhu B. Superior ionic conductivity of Sm^{3+} , Pr^{3+} , and Nd^{3+} triple-doped ceria through bulk and surface two-step doping approach. *Am Chem Soc Appl Mater Interfaces.* 2017;9:23614.

- [14] Omar S, Wachsmann ED, Nino JC. Higher conductivity Sm^{3+} and Nd^{3+} co-doped ceria-based electrolyte materials. *Solid State Ionics*. 2008;178(37–38):1890.
- [15] Ramesh S, Kumar VP, Kistaiah P, VishnuvardhanReddy C. Preparation, characterization and thermo electrical properties of co-doped $\text{Ce}_{0.8-x}\text{Sm}_{0.2}\text{Ca}_x\text{O}_{2-\delta}$ materials. *Solid State Ionics*. 2010;181(1–2):86.
- [16] Ahmed SI, Mohammed T, Bahafi A, Suresh MB. Effect of Mg doping and sintering temperature on structural and morphological properties of samarium-doped ceria for IT-SOFC electrolyte. *Appl Nano Sci*. 2017;7(5):243.
- [17] Pikalova EY, Murashkina AA, Maragou VI, Demin AK, Strelakovsky VN, Tsiakaras PE. CeO_2 based materials doped with lanthanides for applications in intermediate temperature electrochemical devices. *Int J Hydrogen Energy*. 2011;36(10):6175.
- [18] Ji BF, Tian CG, Wang CY, Wu T, Xie JS, Li MH. Preparation and characterization of $\text{Ce}_{0.8}\text{Y}_{0.2-x}\text{Cu}_x\text{O}_{2-\delta}$ as electrolyte for intermediate temperature solid oxide fuel cells. *J Power Sources*. 2015;278:420.
- [19] Ramesh S, Raju KCJ. Preparation and characterization of $\text{Ce}_{1-x}(\text{Gd}_{0.5}\text{Pr}_{0.5})_x\text{O}_2$ electrolyte for IT-SOFCs. *Int J Hydrogen Energy*. 2012;37(13):10311.
- [20] Lin XM, Lu QY, Zhu LL, Liu XM. Synthesis and characterization of $\text{Ce}_{0.8}\text{Sm}_{0.2-x}\text{Pr}_x\text{O}_{2-\delta}$ ($x = 0.02-0.08$) solid electrolyte materials. *J Rare Earths*. 2015;33(4):411.
- [21] Wang FY, Wan BZ, Cheng SF. Study on Gd^{3+} and Sm^{3+} co-doped ceria-based electrolytes. *J Solid State Electrochem*. 2005;9:168.
- [22] Rai A, Mehta P, Omar S. Ionic conduction behavior in $\text{Sm}_x\text{Nd}_{0.15-x}\text{Ce}_{0.85}\text{O}_{2-\delta}$. *Solid State Ionics*. 2014;263:190.
- [23] Venkataramana K, Madhuri C, Reddy YS, Bhikshamaiah G, Reddy CV. Structural, electrical and thermal expansion studies of tri-doped ceria electrolyte materials for IT-SOFCs. *J Alloy Compd*. 2017;719:97.
- [24] Lopez JM, Gilbank AL, Garcia T, Solsona B, Agouramd S, Torrente-Murciano L. The prevalence of surface oxygen vacancies over the mobility of bulk oxygen in nanostructured ceria for the total toluene oxidation. *Appl Catal B*. 2015;174:403.
- [25] Li SP, Lu JQ, Fang O, Luo MF. Effect of oxygen vacancies on electrical properties of $\text{Ce}_{0.8}\text{Sm}_{0.1}\text{Nd}_{0.1}\text{O}_{2-\delta}$ electrolyte: an in situ Raman spectroscopic study. *J Power Sources*. 2009;193(1):93.
- [26] Zhang LL, Liu M, Huang JH, Song ZY, Fu YD, Chang Y, Li CW, He TM. Improved thermal expansion and electrochemical performances of $\text{Ba}_{0.6}\text{Sr}_{0.4}\text{Co}_{0.9}\text{Nb}_{0.1}\text{O}_{3-\delta} - \text{Gd}_{0.1}\text{Ce}_{0.9}\text{O}_{1.95}$ composite cathodes for IT-SOFCs. *Int J Hydrogen Energy*. 2014;39(15):7972.
- [27] Tian CG, Ji BF, Xie JS, Bao WT, Liu K, Cheng JH, Yin QY. Preparation and characterization of $\text{Ce}_{0.8}\text{La}_{0.2-x}\text{Y}_x\text{O}_{1.9}$ as electrolyte for solid oxide fuel cells. *J Rare Earths*. 2014;32(12):1162.
- [28] Prashanth Kumar V, Reddy YS, Kistaiah P, Prasad G, Reddy CV. Thermal and electrical properties of rare-earth co-doped ceria ceramics. *Mater Chem Phys*. 2008;112:711.
- [29] Prekajski M, Stojmenovic M, Radojkovic A, Brankovic G, Oraon H, Subasri R, Matovic B. Sintering and electrical properties of $\text{Ce}_{1-x}\text{Bi}_x\text{O}_{2-\delta}$ solid solution. *J Alloy Compd*. 2014;617:563.
- [30] Tadokoro SK, Muccilo ENS. Effect of Y and Dy co-doping on electrical conductivity of ceria ceramics. *J Eur Ceram Soc*. 2007;27(13–15):4261.
- [31] Shannon RD. Revised effective ionic radii and systematic studies of interatomic distances in halides and chalcogenides. *Acta Cryst*. 1976;A32:751.
- [32] Chrystian GM, Santos TH, Ricardo JPG, Dutra PS, Nascimento RM, Rajesh S, Fonseca FC, Macedo DA. Synthesis and properties of CuO-doped $\text{Ce}_{0.9}\text{Gd}_{0.1}\text{O}_{2-\delta}$ electrolytes for SOFCs. *Ceram Int*. 2015;41(3):4161.
- [33] Chaubey N, Wani BN, Bharadwaj SR, Chattopadhyaya MC. Physicochemical properties of rare earth doped ceria $\text{Ce}_{0.9}\text{Ln}_{0.1}\text{O}_{1.95}$ ($\text{Ln} = \text{Nd, Sm, Gd}$) as an electrolyte material for IT-SOFC/SOEC. *Solid State Sci*. 2012;20:135.
- [34] Zhan ZL, Wen TL, Tu HY, Lu ZY. AC impedance investigation of samarium-doped ceria. *Electrochem Soc*. 2001;148(5):A427.
- [35] Matovic B, Stojmenovic M, Pantic J, Varela A, Zunic M, Jiraborvornpongsa N, Yano T. Electrical and microstructural properties of Yb-doped CeO_2 . *J Asian Ceram Soc*. 2014;2:117.
- [36] Payne RU, Zhu Y, Zhu WH, Timper MS, Elangovan S, Tatarchuk BJ. Diffusion and gas conversion analysis of solid oxide fuel cells at loads via AC impedance. *Int J Electrochem*. 2011. <https://doi.org/10.4061/2011/465452>.
- [37] Ravi Chandran P, Arjunan TV. Investigation on Mg and Sc co-doped Ceria electrolyte for IT-SOFC. *Int J Eng Technol*. 2014;6(3):1432.
- [38] Hayashi H, Kanoh M, Quan CJ, Inaba H, Wang SR, Dokiya M, Tagawa H. Thermal expansion of Gd-doped ceria and reduced ceria. *Solid State Ionics*. 2000;132(3–4):227.
- [39] Venkatesh V, Kumar VP, Sayanna R, Reddy CV. Preparation, characterization and thermal expansion of Pr Co-dopant in samarium doped ceria. *Adv Mater Phys Chem*. 2012;2:5.
- [40] Zheng YF, He SC, Ge L, Zhou M, Chen H, Guo LK. Effect of Sr on Sm-doped ceria electrolyte. *Int J Hydrogen Energy*. 2011;36(8):5128.
- [41] Kong X, Liu GY, Yi ZZ, Ding XF. $\text{NdBaCu}_2\text{O}_{5+\delta}$ and $\text{NdBa}_{0.5}\text{Sr}_{0.5}\text{Cu}_2\text{O}_{5+\delta}$ layered perovskite oxides as cathode materials for IT-SOFCs. *Int J Hydrogen Energy*. 2015;40(46):16477.
- [42] Jin C, Yang ZB, Zhang HH, Yang CH, Chen FL. $\text{La}_{0.6}\text{Sr}_{1.4}\text{MnO}_4$ layered perovskite anode material for intermediate temperature solid oxide fuel cells. *Electrochem Commun*. 2012;14(1):75.
- [43] Yaremchenko AA, Brinkmann B, Janssen R, Frade JR. Electrical conductivity, thermal expansion and stability of Y- and Al-substituted SrVO_3 as prospective SOFC anode material. *Solid State Ionics*. 2013;247–248:86.
- [44] Vibhu V, Rougier A, Nicollet C, Flura A, Grenier JC, Bassat JM. $\text{La}_{2-x}\text{Pr}_x\text{NiO}_{4+\delta}$ as suitable cathodes for metal supported SOFCs. *Solid State Ionics*. 2015;278:32.